energies

MDPI

Article

Modeling of Working Machines Synergy in the Process of the Hybrid Electric Vehicle Acceleration

Konrad Prajwowski, Wawrzyniec Golebiewski *, Maciej Lisowski, Karol F. Abramek and Dominik Galdynski

Department of Automotive Engineering, Faculty of Mechanical Engineering and Mechatronics, West Pomeranian University of Technology, Piastow Avenue 19, 70-310 Szczecin, Poland; kprajwowski@zut.edu.pl (K.P.); mlisowski@zut.edu.pl (M.L.); kabramek@zut.edu.pl (K.F.A.); dgaldynski@zut.edu.pl (D.G.)

* Correspondence: wgolebiewski@zut.edu.pl; Tel.: +48-914494874

Received: 7 October 2020; Accepted: 3 November 2020; Published: 6 November 2020

Abstract: There are many different mathematical models that can be used to describe relations between energy machines in the power-split hybrid drive system. Usually, they are created based on simulations or measurements in bench (laboratory) conditions. In that sense, however, these are the idealized conditions. It is not known how the internal combustion engine and electrical machines work in real road conditions, especially during acceleration. This motivated the authors to set the goal of solving this research problem. The solution was to implement and develop the model predictive control (MPC) method for driving modes (electric, normal) of a hybrid electric vehicle equipped with a power-split drive system. According to the adopted mathematical model, after determining the type of model and its structure, the measurements were performed. There were carried out as road tests in two driving modes of the hybrid electric vehicle: electric and normal. The measurements focused on the internal combustion engine and electrical machines parameters (torque, rotational speed and power), state of charge of electrochemical accumulator system and equivalent fuel consumption (expressed as a cost function). The operating parameters of the internal combustion engine and electric machines during hybrid electric vehicle acceleration assume the maximum values in the entire range (corresponding to the set vehicle speeds). The process of the hybrid electric vehicle acceleration from 0 to 47 km/h in the electric mode lasted for 12 s and was transferred into the equivalent fuel consumption value of 5.03 g. The acceleration of the hybrid electric vehicle from 0 to 47 km/h in the normal mode lasted 4.5 s and was transferred to the value of 4.23 g. The hybrid electric vehicle acceleration from 0 to 90 km/h in the normal mode lasted 11 s and corresponded to the cost function value of 26.43 g. The presented results show how the fundamental importance of the hybrid electric vehicle acceleration process with a fully depressed gas pedal is (in these conditions the selected driving mode is a little importance).

Keywords: modeling; acceleration; hybrid electric vehicle; engine; generator; motor

1. Introduction

The effective synergy of the internal combustion engine and electrical machines, as well as the use of energy recovery during recuperative braking, allows the hybrid electric vehicle (HEV) to reduce its fuel consumption. Another undoubted advantage associated with the greater energy efficiency is the lower level of toxic emissions [1,2]. The improvement of economic and ecological indicators depends on an effective energy management system. To date, various models of power flow management strategies have been used in hybrid electric vehicles. Early energy management systems were based on the predicted operating conditions of the hybrid electric vehicle drive system (heuristic hypotheses).

Control strategy of the internal combustion engine and electric engine operation assumed the use of electric mode from the state of the stationary car to the given vehicle speed. Above this speed, the torque of the electric motor decreased, and the shortage of torque, to overcome the resistance to movement, was gratified by the internal combustion engine [3,4]. The priority of the energy management system was to minimize the performance indicator described as the mass of fuel consumed in time [5–7].

Barsali et al. proposed statistical optimization as an energy management strategy based on minimizing the fuel consumption [5]. This approach did not require the detailed knowledge of the actual power demand, but only the knowledge of its average value. The accuracy of the method used resulted in its development in an energy management strategy for the electric power system ensuring reduction of fuel consumption and toxic emissions, based on dynamic programming (DP) [8–11]. The concept presented by Lin et al. [10] was based on stochastic-dynamic programming (SDP). The authors' approach assumed a deterministic vehicle model, but also a driver's stochastic power demand. The optimization was not based on a specific driving cycle but on the basis of the likelihood of demand for specific power in general driving conditions. Due to the considerable computational time requirements, the numerical optimization methods have been replaced by analytical optimization methods [3,12]. The method limiting the calculation expenditure assumed the introduction of the Hamiltonian function. The energy management strategy also used the theory of optimal control described by the Euler–Lagrange equation.

A different approach to the topic of energy management in hybrid vehicles could be found in the works of Paganelli et al. [13,14]. They present algorithms for the equivalent consumption minimization strategy (ECMS) for both hybrid drive systems and hybrid electric vehicles equipped with fuel cells. The strategy for controlling the value of equivalent fuel consumption was also used in the literature [15,16] and was presented as a cost function defined in the form of the sum of fuel and electricity consumption. This value, however, depended on a priori information on driving conditions or on the conditions of the adopted driving cycle. The modification of the ECMS optimization algorithm used for power-split hybrid systems was undertaken by Liu and Peng [17]. They used the SDP and ECMS strategy and the algorithms they used allowed them to improve the dynamic properties of the hybrid electric vehicle while reducing fuel consumption. They also built an automatic model of the power-split hybrid system in which the applied methodology proposed the automatic generation of dynamic systems equations. The algorithms show the cooperation of the internal combustion engine with electric machines, ensuring lower fuel consumption (as part of experiments according to a specific driving cycle) [18].

Another real-time algorithm used for decreasing the fuel consumption was the particle swarm optimization (PSO) [19–24]. This method has been applied in hybrid electric vehicles (HEVs) and plug-in HEVs [19,20]. The main goal of the algorithm was to optimize the control strategy in order to achieve the lowest fuel consumption. The development of the algorithm used by Hwang and Chen improved the fuel consumption by 9.4% in relation to the base control model [24].

Earlier Kim et al. [25] developed another energy management system in hybrid vehicles called the model predictive control (MPC). It was a strategy for optimal torque distribution for a parallel hybrid drive system. The cost function used in it was minimized on the basis of telemetric estimation of the vehicle speed. Borhan et al. [26] used the MPC in a power-split hybrid drive system equipped with an ultra-capacitor as the energy storage system. In parallel, Moura et al. [27] developed supervision to minimize the fuel consumption of a vehicle equipped with a series hybrid drive system by stochastic optimization of the control process using the Markov chain.

The MPC method was also used to determine the control inputs for economic driving (better fuel economy) of HEVs [28] and it depended largely on information from the management of Intelligent Transportation System (ITS). Yang and Zhu [29,30] developed the MPC system using linear quadratic tracking (LQT) consisting of controlling the power distribution of a power-split hybrid system to track the expected power demand set by a driver. The LQT controller minimized the cost function and at the same time maintained the battery level at the desired level.

An alternative development of the MPC strategy was the use of an energy management system known as nonlinear model predictive control (NMPC). The method used allowed an improvement in the amount of fuel consumption obtained in the NEDC cycle by 8.8% (compared to the factory control of the power-split hybrid system) [31].

The model of power-split hybrid systems was also presented by Cao, Peng and He. It was characterized by high accuracy; however, the created model was tested experimentally based on specific driving cycles, such as the new european driving cycle (NEDC) or the highway fuel economy driving schedule (HWYCOL) [32].

The above literature review brings the current state of knowledge related to the different mathematical models of the power-split hybrid drive system. They were created based on simulations or observations and measurements in bench (laboratory) conditions [17,18,29–32]. In the sense; however, these are idealized conditions. It is not known how the internal combustion engine and electrical machines work in real road conditions, especially during acceleration in various driving modes. It is not known whether the selection of the driving mode is of a significance importance during acceleration. It is also unknown in which driving mode the acceleration of the hybrid electric vehicle is more energy efficient. Those scientific considerations led the authors to set the goal of solving this research problem. The solution to the research problem was the implementation and development of the MPC method for driving modes (electric, normal) of a hybrid electric vehicle equipped with a power-split drive system. It was carried out in accordance with the research program, which assumed:

- specification of the components assembled in the tests (experimental part);
- creating a mathematical model of a power-split hybrid vehicle;
- presentation of the results;
- discussion of the results and conclusions.

2. Experimental Part

The experiments included the identification of the test object, a polygon stand and the test apparatus. The test object was a third generation Toyota Prius vehicle. The basic vehicle parameters are summarized in Table 1a,b [19,33].

The polygon stand was an asphalt road located outside the city. The operation parameters of the internal combustion engine and electric machines have been tested using the test equipment (Gutmann Mega Macs diagnostic program and Dynomet chassis dynamometer). The specific results of the given parameters were obtained in Section 4.

Table 1. (a) Vehicle parameters; **(b)** Vehicle parameters.

(a)	
Total mass	1630 kg (1445 kg + 185 kg—driver and passenger)
Dynamic wheel radius	0.29 m
Frontal area	1.62 m^2
Rolling resistance coefficient	0.0084—tire energy class C
Air drag coefficient	0.25
Drive system type HEV	power-split hybrid
Internal Combustion Engine Specification	
Ignition type	spark ignition
Capacity	1.8 dm^3
Number of cylinders	4
Max. power	73 kW
Max. power rotational speed	5200 rpm
Max. torque	142 Nm

Table 1. *Cont.*

(b)	
Max. torque rotational speed	4000 rpm
Mass moment of inertia	0.18 kg m^2
Generator (MG1) Specification	
Type	three-phase synchronous alternating current (AC)
Function	generator, internal combustion engine (ICE) starter
Rated voltage	500 V
Maximum output power	42 kW
Max torque	45 Nm
Current at max torque	75 A
Max. rotational speed	10,000 rpm
Mass moment of inertia	0.023 kg m^2
Electric Motor (MG2) Specification	
Type	three-phase synchronous AC
Function	generator, wheel drive
Rated voltage	500 V
Maximum output power	60 kW
Maximum torque	207 Nm
Current at max torque	230 A
Max. rotational speed	13,000 rpm
Mass moment of inertia	0.012 kg m^2
High Voltage Battery and Inverter Specification	
Battery type	NiMH
Nom. voltage	201.6 V
Capacity	6.5 Ah

3. Model of a Power-Split Hybrid Drive System

A model of a power-split electric-combustion drive system is shown in Figure 1. It consists of the following components: traffic conditions (desired speed), driver, driving modes, gas pedal, powertrain controller, internal combustion engine, generator, electric motor, high voltage battery, inverter, planetary gear, main gear, wheels and current speed. The driver, who selects the operating mode of the system (electric, normal) and presses on the gas pedal which transfers into the power of the vehicle (the power demand is stochastic), is the variable controlling the hybrid system. The drive system controller receives signals from a series of sensors, which include, among others, gas pedal position sensors and wheel speed sensor, and monitors the operation of the vehicle with the implemented energy management system.

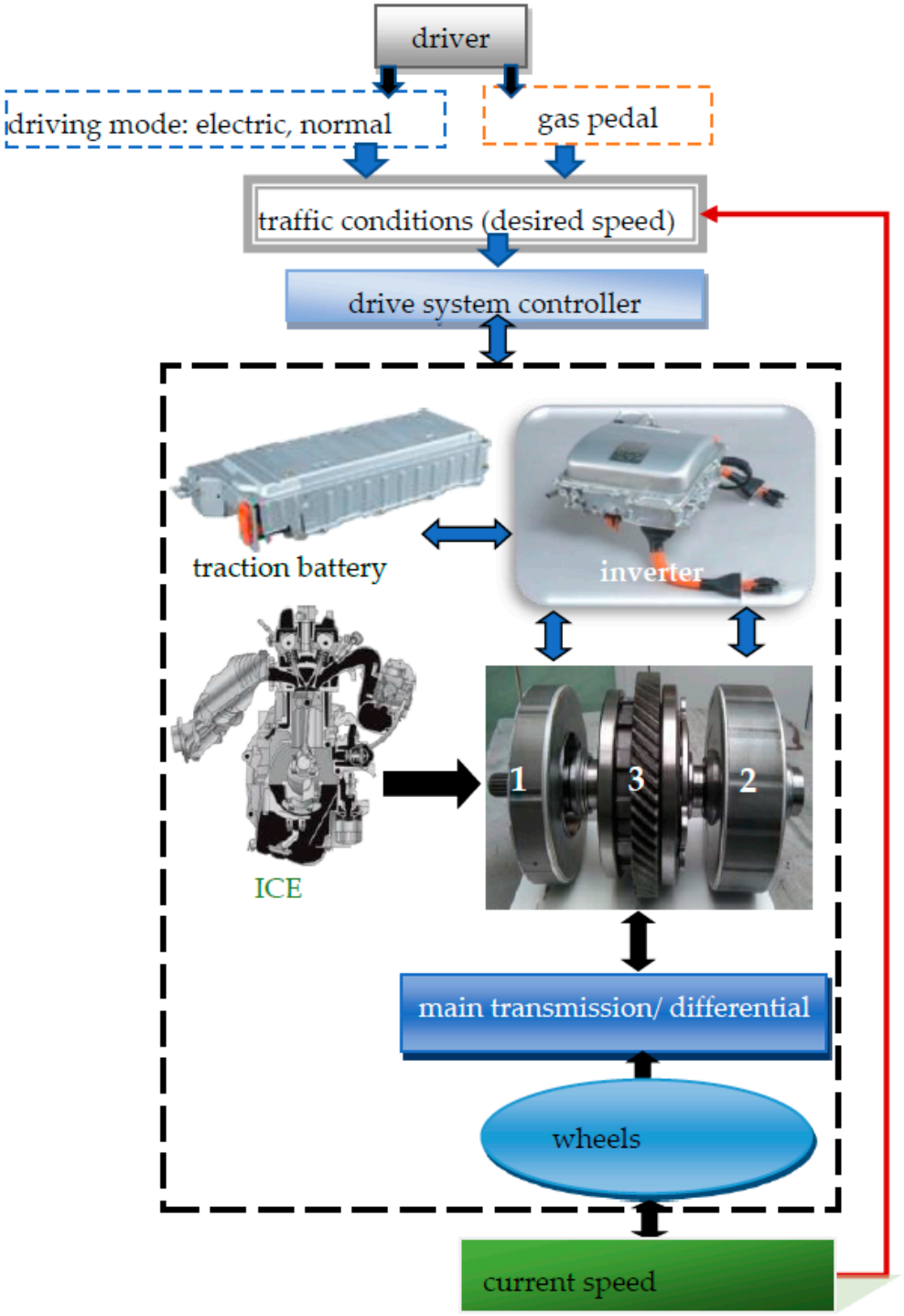

Figure 1. Construction of the power-split hybrid drive model: ICE—internal combustion engine, 1—generator (MG1), 2—electric motor (MG2), 3—planetary gear set.

3.1. Torque Transmission Dynamics and Vehicle Movement

The third generation Toyota Prius vehicle is equipped with two planetary gears. The kinematic diagram of the system for the normal driving mode is shown in Figure 2. The torque generated by the internal combustion engine is transmitted to the yoke of the satellite wheels and then to the ring gear of the planetary gear.

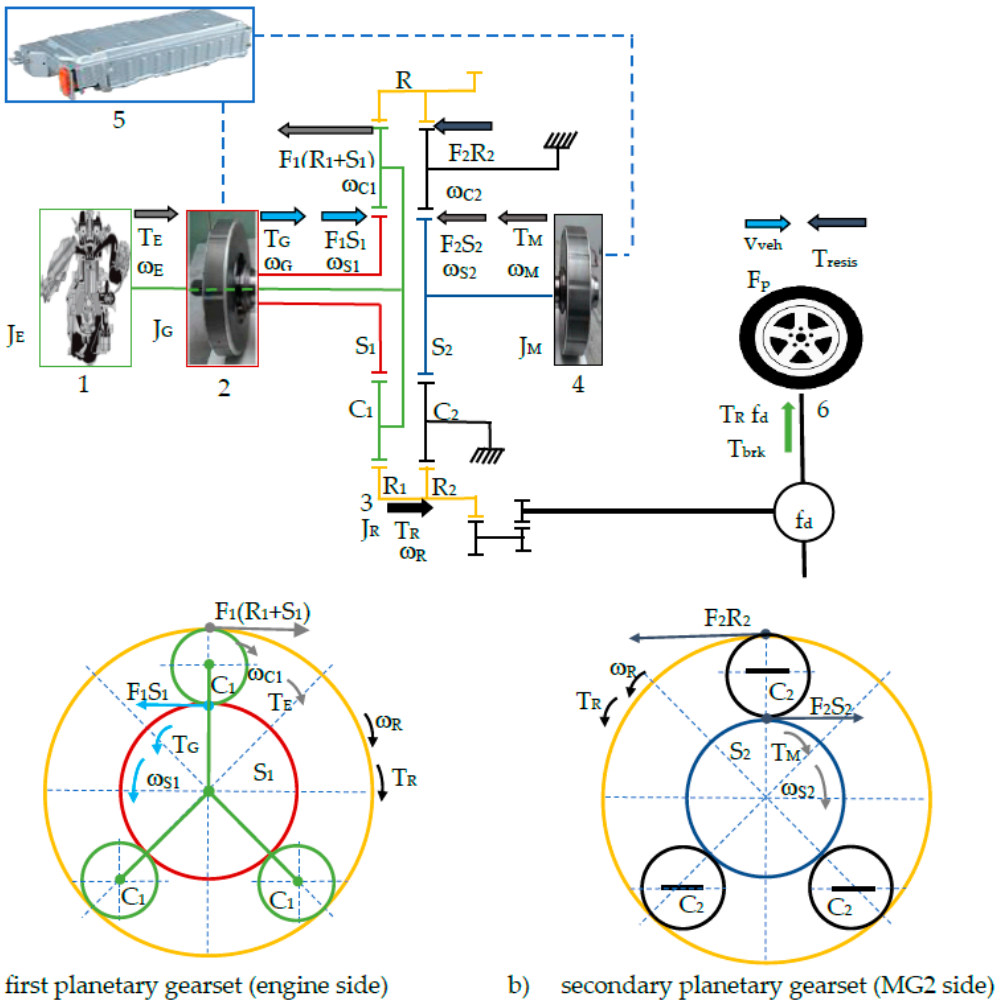

Figure 2. Torque transmission dynamics model (normal driving mode): 1—combustion engine, 2—MG1 electric machine (starter, generator), 3—planetary gear assembly, 4—MG2 electric machine (electric motor, generator), 5—traction battery, 6—wheels.

After the transmission through the planetary gear, the torque, using the intermediate gear and main gear, drives the car's axle shafts. The MG1 generator, connected to the sun gear, acts as a starter and is used to charge the battery while driving. The MG2 electric machine, connected to the sun gear of the second planetary gear (transferring torque to the ring gear by the immobilized satellite yoke) was designed to assist the internal combustion engine in generating power, but also to provide energy recovery during braking [33].

In order to implement the mathematical model describing the dynamic scheme of torque transmission in the power-split hybrid drive system, the following assumptions were made:

- all shaft connections are rigid so there is no slippage between the drive components (no power loss);
- the moments of inertia of the internal combustion engine and electric machines are related to the moments of inertia of the yokes of satellites, sun wheels and crown gear;
- the moment of inertia of the main gear pinion is not taken into account;
- only longitudinal forces acting on the vehicle during travel are taken into account.

The drive system model (Figure 2) for the normal driving mode is described by the following equations [33]:

(a) Angular velocities:

$$\omega_{C1} = \frac{R_1}{S_1 + R_1}\omega_R + \frac{S_1}{S_1 + R_1}\omega_{S1} \quad (1)$$

$$\omega_{C2} = \frac{R_2}{S_2 + R_2}\omega_R + \frac{S_2}{S_2 + R_2}\omega_{S2} \tag{2}$$

The yoke of the satellites of the second planetary gear is locked, therefore $\omega_{C2} = 0$.

$$0 = \frac{R_2}{S_2 + R_2}\omega_R + \frac{S_2}{S_2 + R_2}\omega_{S2} \tag{3}$$

$$\frac{R_2}{S_2 + R_2}\omega_R = -\frac{S_2}{S_2 + R_2}\omega_{S2} \tag{4}$$

$$\omega_R = -\frac{S_2}{R_2}\omega_{S2} \tag{5}$$

$$\omega_{S2} = \omega_M, \omega_{C1} = \omega_E, \omega_{S1} = \omega_G \tag{6}$$

$$\omega_R = -\frac{S_2}{R_2}\omega_M \tag{7}$$

$$\omega_E = \frac{R_1}{S_1 + R_1}\omega_R + \frac{S_1}{S_1 + R_1}\omega_G \tag{8}$$

$$\omega_E = -\frac{R_1}{S_1 + R_1} \cdot \frac{S_2}{R_2}\omega_M + \frac{S_1}{S_1 + R_1}\omega_G \tag{9}$$

$$\omega_M = -\frac{R_2}{S_2}\omega_R \tag{10}$$

$$\omega_G = \frac{\omega_E(R_1 + S_1)}{S_1} + \frac{R_1}{S_1}\frac{S_2}{R_2} \cdot \omega_M \tag{11}$$

(b) Mass moments of inertia and torques of the system:

$$J_E \cdot \dot{\omega_E} = T_E - F_1(R_1 + S_1) \tag{12}$$

$$J_G \cdot \dot{\omega_G} = T_G + F_1 S_1 \tag{13}$$

$$J_M \cdot \dot{\omega_M} = T_M - F_2 S_2 \tag{14}$$

$$J_R \cdot \dot{\omega_R} = F_1 R_1 + F_2 R_2 - T_R = \frac{R_1}{R_1 + S_1}T_E + \frac{R_2}{S_2} \cdot T_M - T_R \tag{15}$$

(c) Vehicle inertia:

$$m \cdot \dot{v_{veh}} = \frac{T_R f_d + T_{brk}}{r_d} - \frac{1}{2}\rho_A \cdot C_d A_f v_{veh}^2 - mg(f_r cos\alpha + sin\alpha) \tag{16}$$

(d) Vehicle speed:

$$v_{veh} = \frac{\omega_R \cdot r_d}{f_d} \tag{17}$$

Using the equations from (1) to (17) with the above-mentioned assumptions ($J_R \approx 0$) the simplified version of the model is as follows:

$$\left[J_E + J_G\left(\frac{R_1 + S_1}{S_1}\right)^2\right] \cdot \dot{\omega_E} - \left[J_G \frac{R_1 \cdot S_2 \cdot (R_1 + S_1)}{R_2 \cdot S_1^2}\right] \cdot \dot{\omega_M} = T_E + T_G \cdot \frac{(R_1 + S_1)}{S_1} \tag{18}$$

$$\left[J_E \cdot \frac{R_1}{R_1+S_1}\right]\dot{\omega}_E + \left[J_M \frac{R_2}{S_2} - m \cdot \left(\frac{r_d}{f_d}\right)^2 \cdot \frac{S_2}{R_2}\right] \cdot \dot{\omega}_M = T_E \cdot \frac{R_1}{R_1+S_1} + T_M \cdot \frac{R_2}{S_2} + \frac{T_{brk}}{f_d} + \frac{1}{2} \cdot \rho_A \cdot C_d \cdot A_f \cdot \frac{{S_2}^2 \cdot {\omega_M}^2 \cdot r_d^3}{{R_2}^2 \cdot f_d^3} - mg \cdot \frac{r_d}{f_d}(f_r cos\alpha + sin\alpha) \quad (19)$$

The drive system model for the electric mode is described by the following relationships [33]:

(a) Angular velocities:

The first two relations are the same as the (1) and (2) but the yoke of the satellites of the first and second planetary gears is locked, so:

$$0 = \frac{R_1}{S_1+R_1}\omega_R + \frac{S_1}{S_1+R_1}\omega_{S1} \quad (20)$$

$$\omega_{S1} = -\frac{R1}{S_1} \cdot \omega_R \quad (21)$$

$$0 = \frac{R_2}{S_2+R_2}\omega_R + \frac{S_2}{S_2+R_2}\omega_{S2} \quad (22)$$

$$\frac{S_2}{S_2+R_2}\omega_{S2} = -\frac{R_2}{S_2+R_2}\omega_R \quad (23)$$

$$\omega_R = -\frac{S_2}{R_2}\omega_{S2} \quad (24)$$

$$\omega_{S1} = \omega_G, \omega_{S2} = \omega_M \quad (25)$$

$$\omega_R = -\frac{S_2}{R_2}\omega_M \quad (26)$$

$$\omega_E = 0 \quad (27)$$

$$\omega_G = -\frac{R}{S_1} \cdot \omega_R = \frac{R}{S_1}\frac{S_2}{R_2}\omega_M \quad (28)$$

(b) Mass moments of inertia and torques of the system ($J_E = 0$, $T_E = 0$):

$$J_G \cdot \dot{\omega}_G = T_G + F_1 S_1 \quad (29)$$

$$J_M \cdot \dot{\omega}_M = T_M - F_2 S_2 \quad (30)$$

$$J_R \cdot \dot{\omega}_R = F_2 R_2 - T_R = \frac{R_2}{S_2} \cdot T_M - T_R \quad (31)$$

$$\left[J_M \cdot \frac{R_2}{S_2} - m \cdot \left(\frac{r_w}{f_d}\right)^2 \cdot \frac{S_2}{R_2}\right]\dot{\omega}_M = T_M \cdot \frac{R_2}{S_2} + \frac{T_{brk}}{f_d} + \frac{1}{2} \cdot \rho_A \cdot C_d \cdot A_f \cdot \frac{{S_2}^2 \cdot {\omega_M}^2 \cdot r_d^3}{{R_2}^2 \cdot f_d^3} - mg \cdot \frac{r_d}{f_d}(f_r cos\alpha + sin\alpha) \quad (32)$$

The inertia and speed of the vehicle have been determined according to the earlier formulas.

3.2. High Voltage Battery Level

The full hybrid drive system model assumed the efficient use of an electricity source (high voltage battery). The state of available electricity is a reflection of the battery charge level, which is determined by the relationship below [16,17,29,30]:

$$SOC = \frac{Q_{max} - Q_{used}}{Q_{max}} \tag{33}$$

The battery capacity used is described by the following relationship:

$$Q_{used} = \begin{cases} \int_0^t I_{bat} \cdot dt \rightarrow discharging,\ propulsion \\ \int_0^t I_{bat} \eta_{coulomb} dt \rightarrow charging,\ recuperation \end{cases} \tag{34}$$

Note that $I_{bat} > 0$ (discharging), $I_{bat} < 0$ (charging). Apart from the charging/discharging current, the influence of uneven charging of individual cells/modules on its SOC should also be taken into account. Modern batteries use the battery charge equalizers (BCE) systems. Their task is to divide the current from the "overcharged" battery cell to the "undercharged" battery cell. This affects the extension of the battery life, but also improves the efficiency of the entire power-split hybrid system (due to the maintenance of a constant electric capacity of the battery). This issue is described in more detail in the literature [34–37]. Next, in correlation to the Equation (34), the derivative of the battery level can be represented by the formula:

$$\dot{SOC} = -\frac{I_{bat}}{Q_{max}} \tag{35}$$

The power of a high-voltage battery:

$$P_{bat} = U_{bus} \cdot I_{bat} = (V_{oc} - I_{bat} \cdot r_{bat}) \cdot I_{bat} = V_{oc} I_{bat} - I_{bat}^2 \cdot r_{bat} \tag{36}$$

Ultimately, the current for charging or discharging the battery takes the form:

$$\dot{SOC} = -\frac{V_{OC} - \sqrt{V_{OC}^2 - 4 r_{bat} P_{bat}}}{2 r_{bat} Q_{max}} \tag{37}$$

The electric power of the P_{bat} battery is used during various driving modes (normal, electric), either during drive or recuperation, to cover the demand for power generated by the generator and/or the electric motor according to the following equation:

$$P_{bat} = T_G \cdot \omega_G + T_M \cdot \omega_M = T_{des} \omega_M - T_E \cdot \omega_E \tag{38}$$

T_{des} is the torque obtained by pressing the accelerator or brake pedal. It is worth noting that the battery power is positive when it is discharged and negative when it is being charged.

3.3. Energy Management Strategy

At this point the MPC type energy management was used, which allows optimization of the torque distribution value (between the internal combustion engine and electric machines), the substitute fuel consumption at the battery level is maintained as expected. The energy management system is characterized by the following limitations:

(a) Internal combustion engine torque:

$$T_E^{min} \leq T_E \leq T_E^{max} \tag{39}$$

(b) Angular velocity of internal combustion engine:

$$\omega_E^{min} \leq \omega_E \leq \omega_E^{max} \tag{40}$$

(c) Torque of the MG1 electric machine:

$$0 \le T_G \le T_G^{max} \tag{41}$$

(d) Angular speed of the MG1 electric machine:

$$0 \le \omega_G \le \omega_G^{max} \tag{42}$$

(e) Torque of the MG2 electric machine:

$$0 \le T_M \le T_M^{max} \tag{43}$$

(f) Angular speed of the MG2 electric machine:

$$0 \le \omega_M \le \omega_M^{max} \tag{44}$$

(g) High voltage battery power:

$$P_{bat}^{min} \le P_{bat} \le P_{bat}^{max} \tag{45}$$

(h) Battery state of charge:

$$SOC^{min} \le SOC \le SOC^{max} \tag{46}$$

The model described in Sections 3.1 and 3.2 is nonlinear so it has been linearized for specific conditions. The linear version of the model (for the normal and electric driving modes) was presented using the matrix [30]:

$$\begin{bmatrix} E_{11} & -E_{12} \\ E_{21} & E_{22} - \rho_A \cdot C_d \cdot A_f \cdot \dfrac{S_2^2 \cdot r_d^3}{R_2^2 \cdot f_d^3} \end{bmatrix} \cdot \begin{bmatrix} \dot{\omega}_E \\ \dot{\omega}_M \end{bmatrix} = \begin{bmatrix} 1 & \frac{R_1}{R_1+S_1} & 0 \\ \dfrac{R_1}{R_1+S_1} & 0 & \dfrac{R_2}{S_2} \end{bmatrix} \begin{bmatrix} T_E \\ T_G \\ T_M \end{bmatrix} \tag{47}$$

where:

$$E_{11} = J_E + J_G\left(\frac{R_1+S_1}{S_1}\right)^2,\ E_{12} = \left[J_G \frac{R_1 \cdot S_2 \cdot (R_1+S_1)}{R_2 \cdot S_1^2}\right],\ E_{21} = \left[J_E \cdot \frac{R_1}{R_1+S_1}\right],\ E_{22} = \left[J_M \frac{R_2}{S_2} - m \cdot \left(\frac{r_d}{f_d}\right)^2 \cdot \frac{S_2}{R_2}\right]$$

$$E_D = E_{11}\left(E_{22} - \rho \cdot C_d \cdot A_f \cdot \frac{S_2^2 \cdot r_d^3}{R_2^2 \cdot f_d}\right) + E_{12} \cdot E_{21}$$

For the electric driving mode $T_E = 0$, $\omega_E = 0$.

The linearization of the battery charge level to the operating point was then presented in accordance with the following relations [30]:

$$\dot{SOC} = \Gamma_{sG} T_G + \Gamma_{sM} T_M + \Gamma_{s\omega_E} \omega_E + \Gamma_{s\omega_M} \omega_M \tag{48}$$

$$\Gamma_{sG} = \left[\omega_E(R_1+S_1) + \left(\frac{R_1 \cdot S_2}{R_2}\right) \cdot \omega_M\right] / S_1 / \Omega \tag{49}$$

$$\Gamma_{sM} = \omega_M / \Omega \tag{50}$$

$$\Gamma_{s\omega E} = T_G \cdot (R_1+S_1) / S_1 / \Omega \tag{51}$$

$$\Gamma_{s\omega M} = T_M / \Omega \tag{52}$$

$$\Omega = -Q_{max} \sqrt{V_{OC}^2 - 4 r_{bat}\left[T_G \cdot \frac{\left[\omega_E(R_1+S_1) + \left(R_1 \cdot \frac{S_2}{R_2}\right) \cdot \omega_M\right]}{S_1} + T_M \cdot \omega_M\right]} \tag{53}$$

The executive dynamics of the system (internal combustion engine, generator, electric motor) was implemented in accordance with the following relationship [30]:

$$\dot{T}_E = -\frac{T_E}{\tau_E} + \frac{T_{Edes}}{\tau_E}, \dot{T}_G = -\frac{T_G}{\tau_G} + \frac{T_{Gdes}}{\tau_G}, \dot{T}_M = -\frac{T_M}{\tau_M} + \frac{T_{Mdes}}{\tau_M} \tag{54}$$

The relations between the required torque values (internal combustion engine, electric motor) and the system inputs (internal combustion engine fuel consumption and equivalent high voltage battery fuel consumption) have been described using the equations [30]:

$$b = \frac{\dot{m}}{P_E} \tag{55}$$

$$\dot{m} = b \cdot P_E = b \cdot T_{Edes} \cdot \omega_E = \frac{T_{Edes} \cdot \omega_E}{\eta_E \cdot W_u} \tag{56}$$

Calorific value of the fuel (petrol) equaled to 44×10^6 J/kg. The equivalent fuel consumption (calculated from the energy consumed from a high-voltage battery) was determined from the following formula:

$$\dot{m}_{eq} = C_{bat} \cdot P_{bat} = C_{bat} \cdot V_{oc} \cdot I_{bat} \tag{57}$$

Finally, it took the form:

$$\dot{m}_{eq} = \frac{C_{bat}}{2r_{bat}}\left[V_{oc}^2 - V_{oc} \cdot \sqrt{V_{oc}^2 - 4r_{bat}P_{bat}}\right] \tag{58}$$

The value of the equivalent energy consumption coefficient C_{bat} for batteries has been calculated and it was equal to 0.0000227. It was determined on the basis of the equivalent fuel consumption (the ratio of the battery power to the calorific value of the fuel). In accordance with the literature [16] the value of the coefficient b1 was adopted and the values of the a1 coefficient have been calculated (from 0.0000227 to 0.0000237).

The main purpose of the presented energy management system was to minimize the fuel consumption of the internal combustion engine and the equivalent fuel consumption (corresponding to the energy consumption of the high-voltage battery). The parameter describing these relationships was the cost function presented according to the formula [17]:

$$J = \sum\nolimits_{s=0}^{N-1} (fuel_s + \alpha_E \Delta_{SOC}^2) \rightarrow min \tag{59}$$

$$\Delta_{SOC} = \begin{cases} SOC_s - SOC_d \; SOC_s < SOC_d \\ 0 \; SOC_k \geq SOC_d \end{cases} \tag{60}$$

Using the previous relationships, the cost function can assume the following form:

$$J = \int_0^{N \cdot t_d} \rho(\left[\dot{m}(T_{E\_des}, \tau)\right]^2 + \left[\dot{m}_{eq}(T_{G\_des}, T_{M\_des}, \tau)\right]^2)\Big\} d\tau \rightarrow min \tag{61}$$

Taking into account the expected torque in the cost function, which should correspond to the value of the output torque of the system, the relation (61) takes the form of [17,30]:

$$J = \int_0^{N \cdot t_d} \left[T_{pre}(\tau) - T_R\right]^2 + \rho\left(\left[\dot{m}(T_{E\_des}, \tau)\right]^2 + \left[\dot{m}_{eq}(T_{G\_des}, T_{M\_des}, \tau)\right]^2\right)\Big\} d\tau \rightarrow min \tag{62}$$

Because the cost function is nonlinear, according to the Equation (60), the output control must be converted into categories m and m_{eg}:

$$T_{E\_des} = \frac{\eta_e \cdot W_u}{\omega_E} \cdot \dot{m} \tag{63}$$

The Equations (56) and (58) take the following form:

$$T_{des} = \frac{\dot{m}_{eq}}{C_{bat} \cdot \omega_M} - \frac{r_{bat} \cdot \dot{m}_{eq}{}^2}{V_{oc}^2 \cdot C_{bat}{}^2 \cdot \omega_M} + \frac{T_E \cdot \omega_E}{\omega_M} \tag{64}$$

A linear model of the same operational point is shown below:

$$\dot{T_E} = -\frac{1}{\tau_E} T_E + \Gamma_{e\omega e} \cdot \omega_E + \Gamma_{em} \cdot \dot{m} \tag{65}$$

$$\dot{T_G} = \Gamma_{GTE} \cdot T_E - \frac{1}{\tau_G} T_G \tag{66}$$

$$\dot{T_M} = \Gamma_{MTE} \cdot T_E - \frac{1}{\tau_M} T_M + \Gamma_{M\omega_E} \cdot \omega_E + \Gamma_{M\omega_M} \cdot \omega_M + \Gamma_{Meq} \cdot \dot{m_{eq}} \tag{67}$$

where:

$$\Gamma_{e\omega e} = -\frac{1}{\tau_E} \cdot \frac{\eta_e \cdot W_u \cdot \dot{m_0}}{\omega_{E0}^2}, \; \Gamma_{em} = \frac{1}{\tau_E} \cdot \frac{\eta_e \cdot W_u}{\omega_{E0}} \tag{68}$$

$$\Gamma_{GTE} = -\frac{1}{\tau_G} \cdot \frac{S_1}{R_1 + S_1} \tag{69}$$

$$\Gamma_{MTE} = -\frac{1}{\tau_M} \cdot \left(\frac{R_1}{S_1 + R_1} \cdot \frac{S_2}{R_2} - \frac{\omega_{E0}}{\omega_{M0}} \right) \tag{70}$$

$$\Gamma_{M\omega E} = \frac{1}{\tau_M} \cdot \frac{T_{E0}}{\omega_{M0}} \tag{71}$$

$$\Gamma_{M\omega_M} = -\frac{1}{\tau_M \cdot \omega_{M0}^2} \cdot \left(\frac{\dot{m_{eq0}}}{C_{bat}} - \frac{r_{bat} \cdot \dot{m}_{eq0}^2}{V_{0C}^2 \cdot C_{bat}^2} + T_{E0} \cdot \omega_{E0} \right) \tag{72}$$

$$\Gamma_{M_{eq}} = -\frac{1}{\tau_M \cdot C_{bat} \cdot \omega_{M0}} \cdot \left(1 - 2 \frac{r_{bat}}{V_{0C}^2 \cdot C_{bat}} \right) \tag{73}$$

Then the linear model was a follows:

$$\begin{cases} \dot{x} = A_c x + B_c \boldsymbol{u} \\ y = C_c x + D_c \boldsymbol{u} \end{cases}, \; \boldsymbol{u} = \begin{bmatrix} \dot{m} \\ \dot{m}_{eq} \end{bmatrix} \boldsymbol{y} = T_R \tag{74}$$

where:

$$\boldsymbol{A_c} = \begin{bmatrix} -\frac{1}{\tau_E} & 0 & 0 & \Gamma_{e\omega e} & 0 & 0 \\ \Gamma_{GTE} & -\frac{1}{\tau_G} & 0 & 0 & 0 & 0 \\ \Gamma_{MTE} & 0 & -\frac{1}{\tau_M} & \Gamma_{M\omega E} & \Gamma_{M\omega M} & 0 \\ \frac{E_{22}}{E_D} - \rho \cdot C_d \cdot A_f \cdot \frac{S_2^2 \cdot r_d^3}{R_2^2 \cdot f_d^3 \cdot E_D} + \frac{E_{12}}{E_D}\left(\frac{R_1}{R_1+S_1}\right) & \frac{E_{22}}{E_D} - \rho \cdot C_d \cdot A_f \cdot \frac{S_2^2 \cdot r_d^3}{R_2^2 \cdot f_d^3 \cdot E_D}\left(\frac{R_1}{R_1+S_1}\right) & \frac{E_{12}}{E_D}\frac{R_2}{S_2} & 0 & 0 & 0 \\ -\frac{E_{21}}{E_D} + \frac{E_{11}}{E_D}\left(\frac{R_1}{R_1+S_1}\right) & -\frac{E_{21}}{E_D}\left(\frac{R_1}{R_1+S_1}\right) & \frac{E_{11} \cdot R_2}{E_D \cdot S_2} & 0 & 0 & 0 \\ 0 & \Gamma_{sG} & \Gamma_{sM} & \Gamma_{s\omega e} & \Gamma_{s\omega M} & 0 \end{bmatrix} \tag{75}$$

$$\boldsymbol{x} = \begin{bmatrix} T_E \\ T_G \\ T_M \\ \omega_E \\ \omega_M \\ SOC \end{bmatrix} \tag{76}$$

$$\boldsymbol{B_c} = \begin{bmatrix} \Gamma_{em} & 0 \\ 0 & 0 \\ 0 & \Gamma_{Meq} \\ 0 & 0 \\ 0 & 0 \\ 0 & 0 \end{bmatrix} \tag{77}$$

$$\boldsymbol{C_C^T} = \begin{bmatrix} \frac{R_1}{R_1+S_1} \\ 0 \\ \frac{R_2}{S_2} \\ 0 \\ 0 \\ 0 \end{bmatrix} \tag{78}$$

$$\boldsymbol{C_{CEV}^T} = \begin{bmatrix} 0 \\ 0 \\ \frac{R_2}{S_2} \\ 0 \\ 0 \\ 0 \end{bmatrix} \tag{79}$$

$$\boldsymbol{D_c} = 0 \tag{80}$$

Finally, the linear model takes the form, $\boldsymbol{u}$ and $\boldsymbol{y}$ the same as (74):

$$\begin{aligned} \dot{\boldsymbol{x}} &= A_c x + B_c \boldsymbol{u} \\ \boldsymbol{y} &= C_c x \end{aligned} \tag{81}$$

A further way of solving the problem (using the LQT controller) by converting the analytical model represented by the above equations for the discrete model can be found in the literature [30].

4. Results

The tests scenario was conducted according to the architecture in Figure 3.

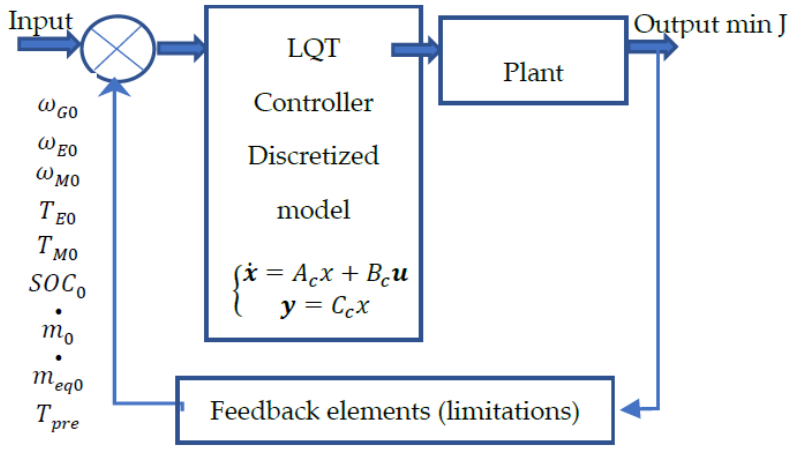

Figure 3. Architecture of the linear quadratic tracking (LQT) algorithm.

The key simulation parameters of the test scenario are summarized in Table 2.

Table 2. Key simulation parameters.

Item	Parameter	Value
Vehicle	Mass	1630 kg
Engine	Start delay	0.5 s
	Time constant	1 s
	Max torque	142 Nm
	Power output	73 kW
Motor	Max torque	207 Nm
	Power output	60 kW
Battery	SOC upper bound	0.75
	SOC lower bound	0.45
	SOC target	0.60

Characteristics of operational parameters of working machines for selected driving modes (normal and electric) based on the tests scenario are presented in Figures 4–7.

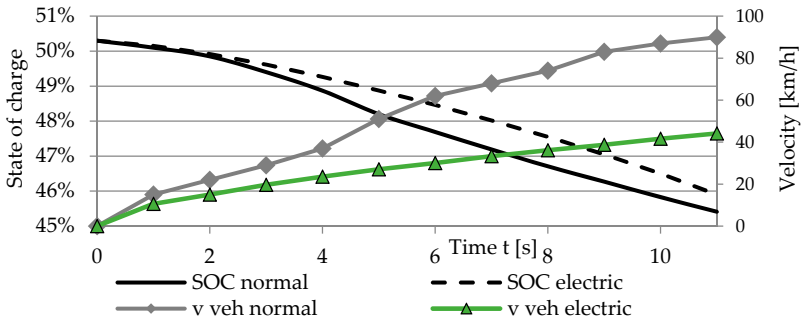

Figure 4. Level of the traction battery charge and vehicle speed versus time.

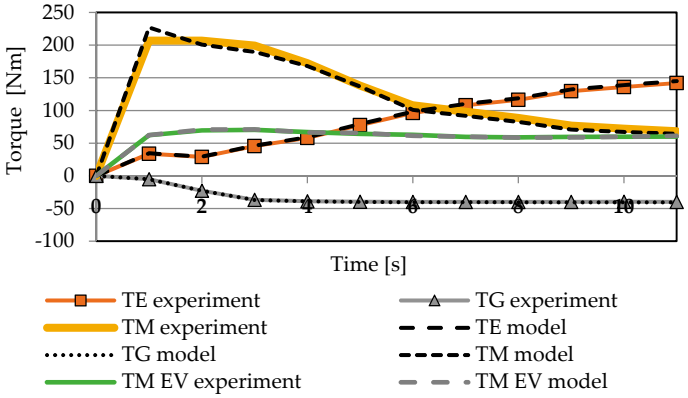

Figure 5. Torque of the internal combustion engine, the electric motor and the generator versus time.

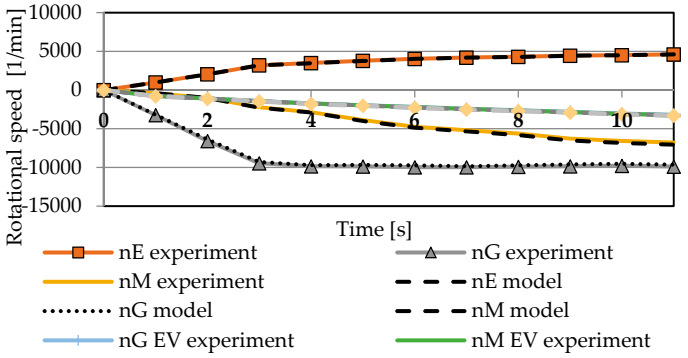

Figure 6. Rotational speed of the internal combustion engine, the electric motor and the generator versus time.

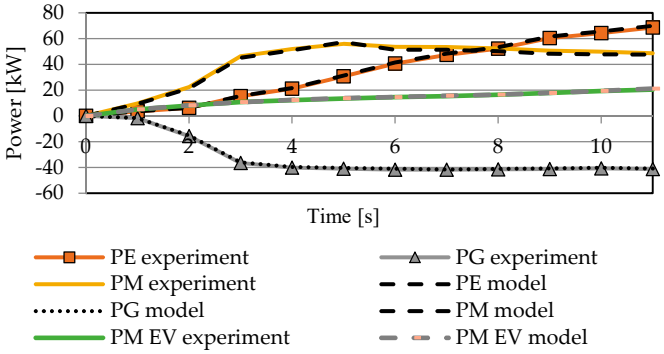

Figure 7. Power of the internal combustion engine, the electric motor and generator on time versus time.

Based on the above characteristics it can be seen that the acceleration of the hybrid electric vehicle in the normal driving mode with the accelerator pedal maximum pressed is spent by a greater decrease in the battery charge level than in the electric driving mode. In the electric mode the vehicle accelerates much slower which is associated with lower energy consumption. While accelerating in the normal driving mode, almost all operational parameters of working machines (torques, powers and rotational speeds) are set within the range of maximum values (corresponding to the given vehicle speed). The situation is different for the electric mode, but this is due to the fact that the driver does not fully press the gas pedal (no maximum power demand). The above considerations also reflect the results of the determined cost function (based on the LQT algorithm) presented below (Figure 8).

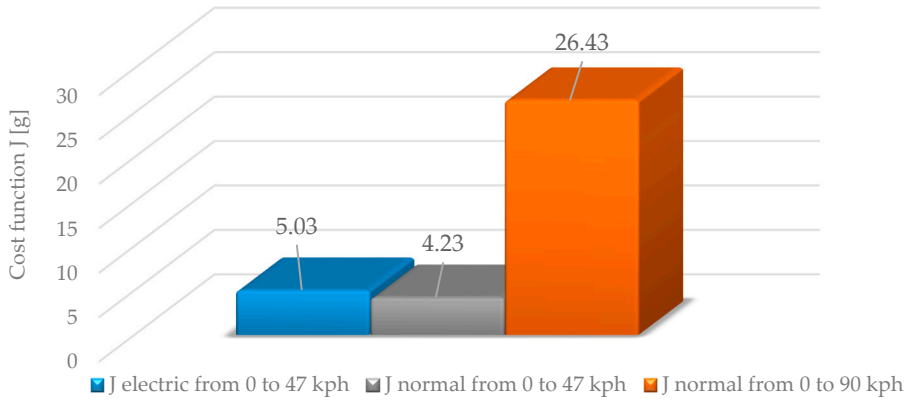

Figure 8. Cost function during acceleration of the vehicle in electric and normal modes (from 0 to 47 km/h and from 0 to 90 km/h).

5. Discussion

The process of accelerating the hybrid electric vehicle from 0 to 47 km/h in electric mode (partial stroke of the accelerator pedal) lasts for 12 s and transfers into the cost function value (equivalent fuel consumption value) of 5.03 g. Accelerating the hybrid electric vehicle from 0 to 47 km/h in normal mode lasts 4.5 s and transfers into the cost function value of 4.23 g. The acceleration of the hybrid electric vehicle from 0 to 90 km/h in normal mode (the accelerator pedal fully pressed) lasts 11 s and corresponds to the value of the cost function of 26.43 g.

Based on Figure 8, it can be concluded that the hybrid electric vehicle accelerates faster in normal mode than in electric mode. Accelerating from 0 to 47 km/h in normal mode takes 7.5 s less than in electric mode (and corresponds to the lower value of the cost function). This demonstrates the importance of the hybrid electric vehicle acceleration process with fully depressed gas pedal (it is the most energy-efficient). In these conditions the selected driving mode is a little importance.

6. Conclusions

The results calculated on the basis of the relationship from the first part of the article prove its high reliability (the accuracy in the vast majority of results reaches 4%). The operating parameters of the internal combustion engine and electric machines during the hybrid electric vehicle acceleration assume the maximum values in the entire range (corresponding to the given car speeds).

The torque values of the internal combustion engine, corresponding to the external characteristic torque values (full power characteristics), correspond to a high efficiency of the entire powertrain of forty percent (the MPC energy management strategy and the LQT controller automatically "sets" the internal combustion engine into the range of a maximum efficiency). This is transferred into low values of the calculated cost function, which actually means lower fuel consumption.

The tests were preliminary; however, in the longer term, the road measurements of the operating parameters of the internal combustion engine and electric machines can be made, as well as the fuel consumption in steady states (constant values of the vehicle speed and torque loading the wheels of the car) and the measurements of the above parameters according to specific driving cycles (NEDC, WLTP, FTP etc.) using bench tests (chassis dynamometer).

Author Contributions: Conceptualization, K.P.; methodology, W.G.; software, M.L.; validation, K.F.A.; formal analysis, D.G.; investigation, W.G.; resources, K.P.; data curation, M.L.; writing—original draft preparation, W.G.; writing—review and editing, W.G.; visualization, M.L.; supervision, K.F.A. All authors have read and agreed to the published version of the manuscript.

Funding: This research received no external funding.

Conflicts of Interest: The authors declare no conflict of interest.

Nomenclatures

A_f	[m^2]	frontal area of vehicle
b	[kg/Ws]	specific fuel consumption
C_d	[-]	air drag resistance coefficient
C_1	[m]	number of teeth of the first set satellites
C_2	[m]	number of teeth of the second set of satellites
f_d	[-]	total gear ratio
f_r	[-]	rolling resistance coefficient
$fuel_s$	[g]	fuel consumption
F_p	[N]	propelling force
F_1	[N]	internal between teeth force of the first gear
F_2	[N]	internal between teeth force of the second gear
g	[ms^{-2}]	gravitational acceleration
I_{bat}	[A]	battery charging/discharging current
J	[g]	cost function
J_E	[kgm^2]	mass moment of inertia of the internal combustion engine
J_G	[kgm^2]	mass moment of inertia of the generator MG1
J_R	[kgm^2]	mass moment of inertia of the planetary gear ring wheel
J_M	[kgm^2]	mass moment of inertia of the electric motor MG2
m	[kg]	total mass of vehicle
$\dot{m}$	[kg/s]	actual fuel consumption
$\dot{m}_{eq}$	[kg/s]	equivalent fuel consumption (high voltage battery flow)
N	[-]	number of steps
P_{bat}	[W]	power of battery
P_E	[W]	internal combustion engine power
Q_{max}	[Ah]	maximum battery capacity
Q_{used}	[Ah]	battery capacity used
r_{bat}	[Ω]	internal battery resistance
r_d	[m]	dynamic wheel radius
R	[m]	number of teeth of the ring gear
R_1	[m]	number of crown wheel teeth
R_2	[m]	number of ring wheel teeth on the electric motor side
s	[-]	step
SOC	[%]	state of charge
SOC_d	[%]	desired state of charge
S_1	[m]	number of teeth of the first sun gear
S_2	[m]	number of teeth of the second sun gear
t	[s]	time
t_d	[-]	jump (step level)
T_{brk}	[Nm]	brake torque
T_{des}	[Nm]	desired torque
T_{Edes}	[Nm]	desired torque of the internal combustion engine
T_{Gdes}	[Nm]	desired torque of the generator
T_{Mdes}	[Nm]	desired torque of the electric motor
T_{pre}	[Nm]	expected system torque
T_{resis}	[Nm]	resistance torque
T_E	[Nm]	torque of the internal combustion engine
T_G	[Nm]	generator torque
T_M	[Nm]	electric engine torque
T_R	[Nm]	torque of the ring gear of the planetary gear
U_{bus}	[V]	voltage in the battery circuit
v_{veh}	[ms^{-1}]	vehicle speed

V_{OC}	[V]	open-circuit voltage of the battery
W_u	[J/kg]	calorific value of fuel
α	[°]	slope of elevation
α_E	[-]	penalty factor
ω_{C1}	[1/s]	angular velocity of the satellite yoke C_1
ω_E	[1/s]	angular speed of the internal combustion engine,
ω_G	[1/s]	angular speed of the generator
ω_M	[1/s]	angular velocity of the electric motor
ω_R	[1/s]	angular velocity of the crown wheel *R* (ring)
ω_{s1}	[1/s]	angular velocity of the sun wheel S1
ω_{s2}	[1/s]	angular velocity of the sun wheel S2
ρ	[-]	coefficient occurring between the tracking error and the equivalent fuel consumption
ρ_A	[kgm^{-3}]	air density
$\eta_{coulomb}$	[-]	Coulomb efficiency
η_E	[-]	overall engine efficiency
τ_E	[s]	internal combustion engine operation time
τ_G	[s]	generator operation time
τ_M	[s]	electric motor operation time

References

1. Ripaccioli, G.; Bernardini, D.; Di Cairano, S.; Bemporad, A.; Kolmanovsky, I.V. A stochastic model predictive control approach for series hybrid electric vehicle power management. In Proceedings of the American Control Conference, Baltimore, MD, USA, 30 June–2 July 2010; pp. 5844–5849.
2. Borhan, H.; Vahidi, A.; Wei, L.; Phillips, A.; di Cairano, S.; Kuang, M.; McGee, R. Nonlinear model predictive control of a power-split hybrid electric vehicle: Influence of inclusion of powertrain dynamics. In Proceedings of the Dynamic Systems and Control Conference, Arlington, VA, USA, 31 October–2 November 2011; pp. 1–8.
3. Kleimaier, A.; Schroder, D. An approach for the online optimized control of a hybrid powertrain. In Proceedings of the 7th International Workshop on Advanced Motion Control, Maribor, Slovenia, 3–5 July 2002; pp. 215–220.
4. Guzzella, L.; Sciarretta, A. *Vehicle Propulsion Systems, Introduction to Modeling and Optimalization*; Springer: Berlin, Germany, 2005; p. 190.
5. Barsali, S.; Miulli, C.; Possenti, A. A control strategy to minimalize fuel consumption of series hybrid electric vehicles. *IEEE Trans. Veh. Technol.* **2004**, *19*, 187–195.
6. Delprat, S.; Lauber, J.; Guerra, T.M.; Rimaux, J. Control of a parallel hybrid powertrain: Optimal control. *IEEE Trans. Veh. Technol.* **2004**, *53*, 872–881. [CrossRef]
7. Musado, C.; Rizzoni, G.; Staccia, B. A ECMS: An adaptive algorithm for hybrid electric vehicle energy management. In Proceedings of the 44th IEEE Conference Decision Control, European Control Conference, Seville, Spain, 12–15 December 2005; pp. 1816–1823.
8. Zhu, Y.; Chen, Y.; Tian, G.; Wu, H.; Chen, Q. A four-step method to design an energy management strategy for hybrid vehicles. In Proceedings of the American Control Conference, Boston, MA, USA, 30 June–2 July 2004; pp. 156–161.
9. Lin, C.C.; Peng, H.; Grizzle, J.W.; Kang, J.M. Power management strategy for a parallel hybrid electric truck. *IEEE Trans. Control Syst. Technol.* **2003**, *11*, 839–849.
10. Lin, C.C.; Peng, H.; Grizzle, J.W. A stochastic control strategy for hybrid electric vehicles. In Proceedings of the American Control Conference, Boston, MA, USA, 30 June–2 July 2004.
11. Back, M. Pradikitive Antriebregulung zum energieoptimalen Betrieb von Hybridfahrzeugen. Ph.D. Dissertation, University Karlsruhe, Karlsruhe, Germany, 2004.
12. Steinmauer, G.; de Re, L. Optimal control of dual power sources. In Proceedings of the 2001 IEEE International Conference on Control Applications, Mexico City, Mexico, 7 September 2001; pp. 422–442.
13. Paganelli, G.; Guezennec, Y.; Rizzoni, G. *Optimizing Control Strategy for Hybrid Fuel Cell Vehicle*; Tech. Rep.; SAE: Warrendale, PA, USA, 2002.
14. Paganelli, G.; Delprat, S.; Guerra, T.; Rimaux, J.; Santin, J. Equivalent consumption minimization strategy for parallel hybrid powertrains. *IEEE Veh. Technol. Conf.* **2002**, *4*, 2076–2081.

15. Sciarretta, A.; Back, M.; Guzzella, L. Optimal control of parallel hybrid electric vehicles. *IEEE Trans. Control. Syst. Technol.* **2004**, *12*, 352–363. [CrossRef]
16. Gao, J.; Zhu, G.; Strangas, E.; Sun, F. Equivalent fuel consumption optimal control of a series hybrid electric vehicle. *Proc. Inst. Mech. Eng. Part D J. Automob. Eng.* **2009**, *23*, 1003–1018. [CrossRef]
17. Liu, J.; Peng, H. Modeling and control of a power-split hybrid vehicle. *IEEE Trans. Control Syst. Technol.* **2008**, *16*. [CrossRef]
18. Liu, J.; Peng, H. Automated modelling of a power-split hybrid vehicles. In Proceedings of the 17th World Congress. The International Federation of Automatic Control, Seoul, Korea, 6–11 July 2008; pp. 4648–4653.
19. Chen, Z.; Xiong, R.; Wang, K.; Jiao, B. Optimal energy management strategy of a plug-in hybrid electric vehicle based on a particle swarm optimization algorithm. *Energies* **2015**, *8*, 3661–3678. [CrossRef]
20. Wu, X.; Cao, B.; Wen, J.; Bian, Y. Particle Swarm Optimization for Plug-in Hybrid Electric Vehicle Control Strategy Parameter. In Proceedings of the 2008 IEEE Vehicle Power and Propulsion Conference, Harbin, China, 3–5 September 2008; pp. 1–5.
21. Abido, M.A. Optimal power flow using particle swarm optimization. *Int. J. Electr. Power Energy Syst.* **2002**, *24*, 563–571. [CrossRef]
22. Chen, Z.; Xiong, R.; Cao, J. Particle swarm optimization-based optimal power management of plug-in hybrid electric vehicles considering uncertain driving conditions. *Energy* **2016**, *96*, 197–208. [CrossRef]
23. Chen, S.-Y.; Hung, Y.-H.; Wu, C.-H.; Huang, S.-T. Optimal energy management of a hybrid electric powertrain system using improved particle swarm optimization. *Appl. Energy* **2015**, *160*, 132–145.
24. Hwang, H.-Y.; Chen, J.-S. Optimized fuel economy control of power—Split hybrid electric vehicle with particle swarm optimization. *Energies* **2020**, *13*, 2278. [CrossRef]
25. Kim, T.S.; Manzie, C.; Sharma, R. Model predictive control of velocity and torque split in a parallel hybrid vehicle. In Proceedings of the IEEE international conference on systems, San Antonio, TX, USA, 11–14 October 2009; pp. 2014–2019.
26. Borhan, H.A.; Vahidi, A. Model predictive control of a power-split hybrid electric vehicle with combined battery and ultra-capacitor energy storage. In Proceedings of the American control conference, Baltimore, MD, USA, 30 June–2 July 2010; pp. 5031–5036.
27. Moura, S.J.; Fathy, H.K.; Callaway, D.S.; Stein, J.L. A stochastic optimal control approach for power management in plug-in hybrid electric vehicles. *IEEE Trans. Veh. Technol.* **2011**, *19*, 545–555. [CrossRef]
28. Yu, K.; Yang, J.; Yamaguchi, D. Model predictive control for hybrid vehicle ecological driving using traffic signal and road slop information. *Control Theory Technol.* **2015**, *13*, 17–28. [CrossRef]
29. Yang, J.; Zhu, G. Adaptive recursive prediction of the desired torque of hybrid powertrain. *IEEE Trans. Veh. Technol.* **2015**, *64*. [CrossRef]
30. Yang, J.; Zhu, G. Model Predictive Control of a Power Split Hybrid Powertrain. In Proceedings of the American Control Conference (ACC), Boston Marriott Copley Place, MA, USA, 6–8 July 2016.
31. Shi, D.H.; Wang, S.H.; Pierluigi, P.; Chen, L.; Wang, R.; Wang, R. Modeling and optimal energy management of a power split hybrid electric vehicle. *Sci. China Tech. Sci.* **2017**, *60*, 713–725. [CrossRef]
32. Cao, J.; Peng, J.; He, H. Modeling and simulation research on power-split hybrid electric vehicle. *Energy Procedia* **2016**, *104*, 354–359. [CrossRef]
33. Merkisz, J.; Pielecha, I. *Uklady Mechaniczne Pojazdow Hybrydowych*; Wydawnictwo Politechniki Poznanskiej: Poznan, Poland, 2015.
34. Ketzer, M.B.; Lima, A.M.N.; Oliveira, A.C.; Jacobina, C.B. Evaluating circuit topologies for battery charge equalization. In Proceedings of the IEEE 39th Annual Conference of the IEEE Industrial Electronics Society, Vienna, Austria, 10–13 November 2013; pp. 743–748.
35. Lin, X.; Stefanopoulou, A.G.; Li, Y.; Anderson, R.D. State of charge imbalance estimation for battery strings under reduced voltage sensing. *IEEE Trans. Control Syst. Technol.* **2015**, *23*, 1052–1062.

36. Ouyang, Q.; Chen, J.; Zheng, J.; Fang, H. Optimal cell-to-cell balancing topology design for serially connected lithium-ion battery packs. *IEEE Trans. Sustain. Energy* **2018**, *9*, 350–360. [CrossRef]
37. Han, W.; Zou, C.; Zhang, L.; Zhou, C. Estimation of cell SOC evolution and system performance in module-based battery charge equalization systems. *IEEE Trans. Smart Grid.* **2019**, *10*, 4717–4727. [CrossRef]